



## SCIENCE OF TSUNAMI HAZARDS

---

Journal of Tsunami Society International

Volume 34

Number 1

2015

---

### AN OCEAN DEPTH-CORRECTION METHOD FOR REDUCING MODEL ERRORS IN TSUNAMI TRAVEL TIME: APPLICATION TO THE 2010 CHILE AND 2011 TOHOKU TSUNAMIS

**Dailin Wang**

NOAA/NWS/Pacific Tsunami Warning Center, 91-270 Fort Weaver Road, Ewa Beach, HI 96706, USA.

[dailin.wang@noaa.gov](mailto:dailin.wang@noaa.gov)

#### ABSTRACT

In this paper, we attempt to reduce the discrepancies between the modeled and observed tsunami arrival times. We treat the ocean as a homogenous fluid, ignoring stratification due to compressibility and variations of temperature and salinity. The phase speed of surface gravity waves is reduced for a compressible fluid compared to that of an incompressible fluid. At the shallow water limit, the reduction in speed is about 0.86% at a water depth of 4000 m. We propose a simple ocean depth-correction method to implement the reduction in wave speed in the framework of shallow water equations of an incompressible fluid: 1) we define an effective ocean depth such that the reduction of the phase speed due to compressibility of seawater is exactly matched by the decrease in water depth (about 2.5% reduction at ocean depth of 6000 m and less than 0.1% at 200 m); 2) this effective depth is treated as if it were the real ocean depth. Implementation of the method only requires replacing the ocean bathymetry with the effective bathymetry so there is no need to modify existing tsunami codes and thus there is no additional computational cost. We interpret the depth-correction method as a bulk-parameterization of the combined effects of physical dispersion, compressibility, stratification, and elasticity of the earth on wave speed. We applied this method to the 2010 Chile and 2011 Tohoku basin-crossing tsunamis. For the 2010 Chile tsunami, this approach resulted in very good agreement between the observed and modeled tsunami arrival times. For the 2011 Tohoku tsunami, we found good agreements between the modeled and the observed tsunami arrival times for most of the DARTs except the farthest ones from the source region, where discrepancies as much as 3-4 min. still remain.

**Keywords:** *tsunami, numerical modeling, shallow water equations, tsunami travel time*

## 1. INTRODUCTION

The destructive February 27, 2010 Chile and March 11, 2011 Tohoku basin-crossing tsunamis were recorded at many ocean bottom pressure sensors, the so-called DART buoys. These tsunamis are generally modeled well by researchers (e.g., Saito et al, 2011; Yamazaki and Cheung 2011; Yamazaki et al. 2012; Grilli et al, 2012). The modeled tsunami arrival times however, are generally too early than the observed at the DARTs by as much as 15 minutes. For the 2010 Chile tsunami, Kato et al. (2011) found that tsunami arrival times at GPS buoys near Japan were as much as 26 minutes later than model predictions.

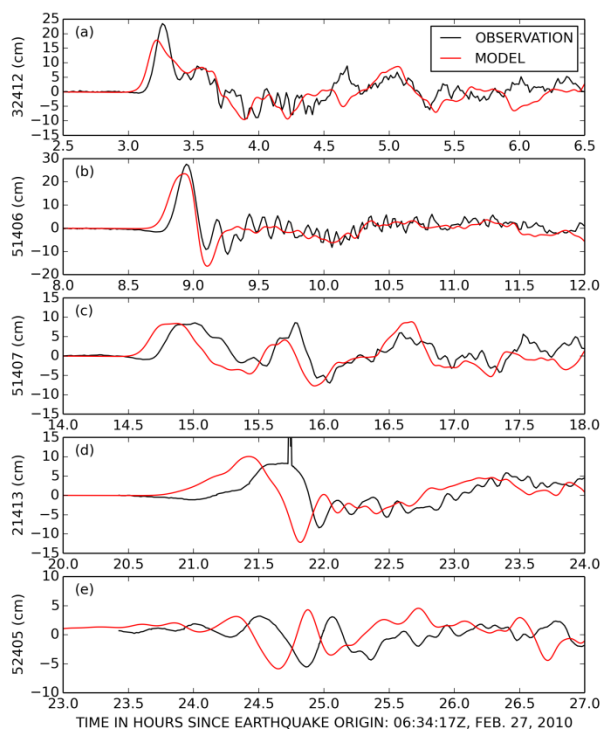


Figure 1. Comparison of RIFT model result with observations at DARTs for the Feb. 27, 2010 Chile tsunami. The model is forced with a rectangular fault with a uniform slip ( $M_w=8.8$ ). This is a post-event rerun extending integration length from 24 to 30 hours. See Section 3.2 for details of the forcing parameters used. The depth-correction method proposed in this study was not applied to this model run.

For the Chile 2010 tsunami, using the real-time tsunami forecast model RIFT (Wang et al., 2009, Wang et al. 2012), the Pacific Tsunami Warning Center (PTWC) was able to predict the wave propagation across the Pacific basin before the nearest DART recorded the tsunami (Foster et al., 2012, supplemental materials). However, the modeled tsunami arrival times were early compared to the observed ones. The discrepancies increased as the distance from the epicenter increased (Figure 1). For DART 21413 near Japan, for example, the predicted arrival time was about 12 minutes earlier

than the observed (Figure 1d). For DART 52405 near Guam, the modeled and observed tsunami waveforms were completely out of phase (Fig. 1e), after 24 hours of propagation.

For the 2011 Tohoku tsunami, Grilli et al. (2012) noted that the modeled tsunami arrival times were earlier than the observed by as much as 15 minutes. Yamazaki et al. (2012) had similar findings. Figure 2 compares the modeled and observed tsunami waveforms at selected DARTs across the Pacific basin. The model result was obtained by forcing the PTWC RIFT model with the USGS finite fault solution (more details are given in section 3.3). Similar to the 2010 Chile tsunami, the differences between modeled and observed tsunami arrival times increased as the distance to the epicenter increased. Seven hours after the earthquake origin, the tsunami arrived at DART 51407 (near Hawaii) about 8 minutes later than predicted (Figure 2b). After 13 hours of propagation, the tsunami arrived at DART 51406 (near Marquesas Islands) about 12 min. later than predicted (Figure 2c). After 20 hours of propagation, the tsunami arrived at DART 32401 (near Chile) about 17 min. later than predicted, with the second peak from the model lining up with the first observed peak (Figure 2e).

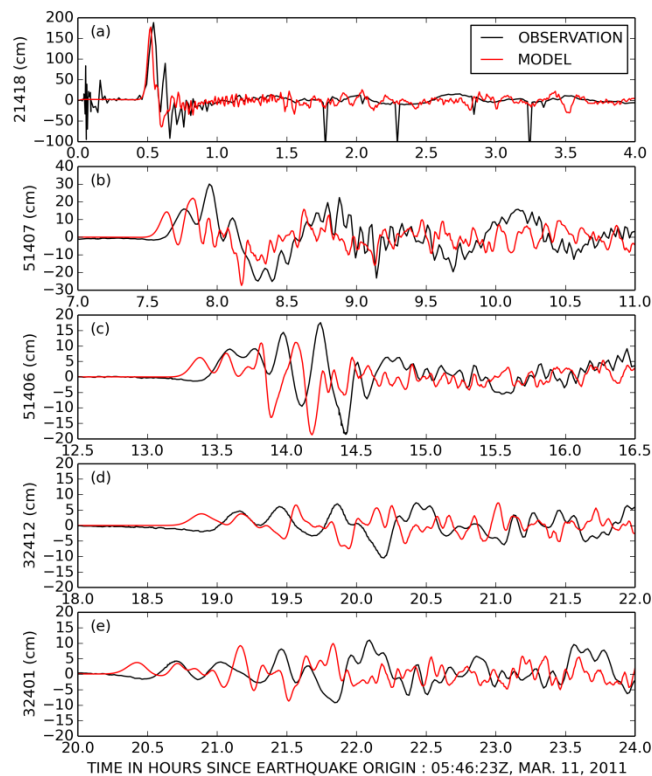


Figure 2. Comparison of RIFT model result without depth-correction with observations at DARTs for the Mar. 11, 2011 Tohoku Tsunami. The model is forced with the USGS finite fault solution ( $M_w=9.0$ ). See Section 3.3 for details of forcing parameters used.

Surface gravity wave phase speed is known to be reduced for a compressible fluid (e.g., Ward 1980, Okal 1982; Yamamoto 1982) and for compressible fluid with background stratification (Shchepetkin and McWilliams 2011). To accurately model the tides, it is known that effects of ocean self-attraction and loading must be included (e.g., Ray 1998). There have been some efforts in trying to explain the discrepancies of the modeled and observed tsunami arrival times (Watada et al. 2011, Tsai et al 2013; Watada 2013). Tsai et al. (2013) found that the total reduction in phase speed is about 1% at 300 km wavelength for an ocean depth of 4000 m, about 0.55% due to density variation of seawater caused by compressibility and dispersion, and 0.45% due to the elasticity of the earth. At 1000 km wavelength, the total reduction in speed is about 1.5%, about 0.5% due to density variation, and 1.0% due to elasticity of the earth (the larger the wavelength, the greater the effect of earth's elasticity has on wave speed). We note that 1000 km wavelength (or 84 min. period at 4000 m water depth) is not a typical characteristic of a damaging tsunami, although spectral analysis might reveal that wavelengths longer than 1000 km contain some energy. It is difficult however, to separate tidal energy and energy due to very long waves of the tsunamis.

Inazu and Saito (2013) introduced a simple parameterization in the shallow water equations to account for the effect of pressure loading on tsunami propagation, using the method of Ray (1998). This is achieved by introducing a small empirical correction (proportional to the surface height) in the pressure gradient term of the momentum equations, in effect reducing the phase speed of the wave propagation. It is shown that the modeled tsunami arrival times agree much better with those of the observed during the 2010 Chile and 2011 Tohoku tsunamis, with an appropriate choice of the empirical parameter related to the correction term. Their method is computationally efficient and can be easily adopted in existing tsunami codes with minimal modification. However, as in the case of tides (Ray 1998), the optimal value of the empirical parameter varies somewhat for different DARTs to achieve the best fit.

Incorporating the effects of density stratification as well as pressure loading, Allgeyer and Cummins (2014) showed that the discrepancies between the modeled and observed tsunami wave times could be drastically reduced. They were also able to reproduce the initial small depression of the leading wave as observed (not present in classical shallow water results). They derived a surface height equation assuming linear density stratification. The resulting equation contains the average density and ocean bottom density, both varying with the depth of the ocean, assuming a linear density profile. The seafloor deformation due to pressure loading is computed using a Green's function approach. Although their method is self-contained and can be used in tsunami forecasting, it is computationally costly, with the computation of the seafloor deformation accounting for 70% of the total model computation time. Watada et al. (2014, also refer to this reference for a more exhaustive discussion of literature on the subject) applied a phase-correction method to solutions of shallow water equations and were able to significantly reduce the tsunami travel time errors at the DARTs and were also able reproduce the small initial depression of the observed tsunamis as well. It is impractical however, to apply their method to the whole computational domain in a nonlinear forward model.

In this study, we attempt to reduce the discrepancies between modeled and observed tsunami arrival times by adopting a simpler approach, starting with the effect of compressibility. We treat the ocean

as a compressible homogenous fluid. The background stratification due to compressibility is ignored (or Boussinesq fluid). The surface gravity wave speed is reduced in such a system (Yamamoto, 1982).

We propose a simple method to implement this new dispersion relation in a shallow water tsunami forecast model, by defining an effective/equivalent ocean depth/bathymetry in a manner that the reduction in phase speed due to compressibility of seawater is exactly matched by the reduction in water depth. The effective ocean depth differs from the true ocean depth by about 2.5% at 6000 m water depth. At water depth less than 200 m, the difference is negligible (less than 0.1%). Implementation of this method is straightforward and there is no need to modify the numerical codes of tsunami forecast models, thus there is no additional computational cost. All that is needed is to replace the real ocean bathymetry with the effective ocean bathymetry, which can be computed once and for all. We call this approach the ocean depth-correction method. We applied this method to the 2010 Chile and 2011 Tohoku tsunamis. The source models used are purely seismic, without any knowledge of the observed tsunami information. With the depth-correction method, we show that the discrepancies between the modeled and the observed tsunami arrival times are greatly reduced.

## 2. Surface gravity wave dispersion relation and method of depth-correction

It is well known that compressibility of seawater reduces the phase speed of surface gravity waves (e.g., Ward 1980; Okal 1982). Here, we start with the dispersion relation of wave motions of a compressible homogenous fluid with a free surface (Yamamoto, 1982):

$$\frac{\omega^2}{k'^2} = \frac{g}{k'} \tanh(k'H), \quad (1)$$

$$\text{where } k'^2 = k^2 - \frac{\omega^2}{s^2}, \quad (2)$$

$k$  is the wave number,  $\omega$  the frequency, and  $s$  the speed of sound in seawater, assumed to be a constant, 1500 m/s.

In the shallow water limit ( $k'H \ll 1$ ), (1) becomes

$$\frac{\omega^2}{k'^2} = gH. \quad (3)$$

Or in terms of the wave number  $k$ ,

$$\frac{\omega^2}{k^2} = gH / (1 + \frac{gH}{s^2}) \quad (4)$$

The dispersion relation (4) is similar to the dispersion relation of classic shallow water surface gravity waves, except it now acquires a factor related to the water depth and sound speed.

We define an effective ocean depth as

$$H_E = H / (1 + \frac{gH}{s^2}) \quad (5)$$

The dispersion relation (4) becomes

$$\frac{\omega^2}{k^2} = gH_E \quad (6)$$

Or the phase speed is

$$C_E = \frac{\omega}{k} = \sqrt{gH_E}. \quad (7)$$

This has the exact form of the classic shallow water wave dispersion relation except the ocean depth is now replaced by an “effective” depth (5). We note that the waves are non-dispersive at the shallow water limit and the phase speed (7) is smaller than the classic shallow water wave speed because

$$\sqrt{\frac{H_E}{H}} < 1,$$

$$C_E = C \sqrt{\frac{H_E}{H}} = C \left( 1 - \frac{gH}{2s^2} + \dots \right), \text{ where } C = \sqrt{gH}, \quad (8)$$

$C$  is the classical shallow water wave phase speed. The second equal sign represents Taylor expansion, for the sake of discussion to follow.

Next we examine the difference between the ocean depth and the effective ocean depth. Figure 3a shows the difference ( $H_E - H$ ) versus the ocean depth  $H$ . At  $H=6000$  m, the difference is 152 m, or 2.5%. At  $H=1000$  m, the difference is 4.3 m, or 0.4%. At  $H=200$  m, the difference is 0.17 m, or less than 0.1%. We note that global ocean bathymetry datasets are usually only accurate to about 1 m. So we can consider differences of order 1 m negligible as far as accuracy of ocean bathymetry for the open ocean is concerned.

Figure 3b shows the percentage difference between the surface gravity wave phase speed  $C_E$  of a compressible ocean with the wave phase speed of incompressible ocean  $C$ . At 6000 m depth, the phase speed reduction due to compressibility is 1.28%. At 4000 m depth, the reduction is 0.86%. At 1000 m, the reduction is 0.22%. Assuming a tsunami wave crosses the Pacific basin in 24 hours at an average ocean depth of 4000 m, the delay of tsunami arrival time will be about 12 minutes.

In Inanzu and Saito (2013), the dispersion relation is

$$C_E = \sqrt{gH(1 - \beta)} = C \left(1 - \frac{\beta}{2} + \dots\right), \quad (9)$$

Where  $\beta$  is tunable parameter and is independent of the water depth. They found that  $\beta = 0.02$ , which amounts to 1% correction in phase speed, gave the best result overall. They did show that different values of  $\beta$  are needed to obtain the best fit for different DARTs.

We should point out that dispersion relation (4) neglects the effect of background stratification due to compressibility. When this effect is taken into account (i.e., for a non-Boussinesq fluid), the dispersion relation will be (to leading order of Taylor expansion):

$$C_E = C \left(1 - \frac{gH}{4s^2}\right), \quad (10)$$

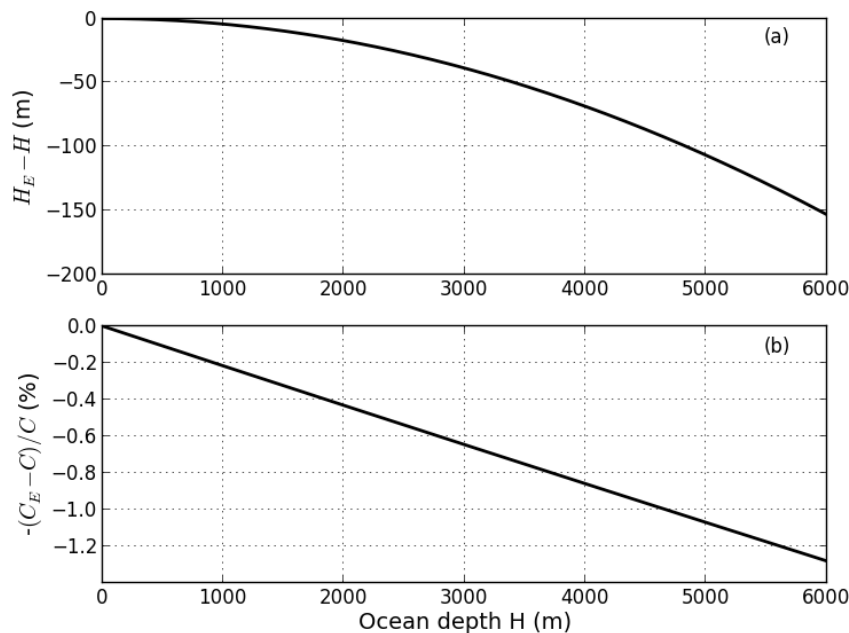


Figure 3. (a) Difference between effective ocean depth defined by equation (5) and true ocean depth; (b) difference between phase speeds of compressible fluid and incompressible fluid, see equation (8).

as derived by Shchepetkin and McWilliams (2011). On the surface, the correction term in equation (4) or equation (8) is off by a factor of two, suggesting (10) should be used. In reality however, the tsunami waves (typical wavelengths of 100-700 km) are weakly dispersive, the shallow water limit is only an approximation. Dispersion alone reduces the wave speed. For example, for a 200 km wavelength at 4000 m depth, the reduction of phase speed is 0.26%. In other words, if a finite wave

number is considered, the difference between (4) and a dispersive version of (10) (see Watada 2013) is not as large as it appears to be for typical tsunami waves. For example, for a 15-min. period wave at 4000 m ocean (180 km wavelength), the phase speed reduction from (4) and from Watada (2013, equation 25) is 0.86% and 0.76% respectively. Only for waves with periods longer than 60 min., does the difference between (4) and that of Watada (2013) approaches to a factor of two.

In light of the fact that elasticity of the earth also reduces the phase speed, we adopt dispersion relation (4) as a “bulk” parameterization, mimicking the combined effects of physical dispersion, compressibility, density variation, and elasticity of the earth on tsunami speed. We call this the depth-correction method. In essence, our approach is similar to the approach of Inazu and Saito (2013) except that our depth correction coefficient is a function of depth and there are no tunable parameters in our approach. In shallow waters the correction is negligible, rather than being a constant fraction everywhere. Implementation of the method is straightforward. All that is needed is to replace the ocean bathymetry with the effective bathymetry (5), thus there is no need to modify existing numerical codes.

### **3. Application to the 2010 Chile and 2011 Tohoku tsunamis**

#### *3.1 The tsunami forecast model and data analysis*

We employ the PTWC real-time linear tsunami forecast model RIFT for this study (Wang et al., 2009; Foster et al., 2012; Wang et al., 2012). The RIFT model solves the linear shallow water equations in spherical coordinates with leap-frog stepping in time and centered difference in space (Arakawa and Lamb, 1977), similar to the linear versions of the tsunami model of Kono et al. (2002) and the real-time tsunami forecast model of Yasuda et al (2013). For bathymetry, we use the GEBCO 30-arc-sec data [Becker et al., 2009], sub-sampled at 4-arc-min. resolution. A 30-hr propagation forecast for the Pacific basin at 4-arc-min. basin can be completed in about 5 min., using a generic 12-CPU Linux server.

The model can take various forms of forcing input. The simplest forcing is a single rectangular fault with a uniform slip of any focal mechanism. The fault length and width are computed according to the empirical formulas of Wells and Coppersmith (1994). The seafloor deformation is computed according to Okada (1985). Following the common practice in tsunami modeling, we assume the ocean is initially at rest (zero velocity) and assume an instantaneous translation of the seafloor deformation to the sea surface. Namely, the initial sea surface deformation takes the same shape as the seafloor deformation. The model can also take finite fault solution as forcing with an arbitrary number of sub-faults. In this case, the Okada (1985) formula of seafloor deformation is computed for each sub-fault and the deformation is instantaneously added to the sea surface elevation at the end of rupture for each sub-fault (or at time = time of rupture + rise time).

The observed tsunami data at the DARTs are processed to remove the tides. This is done by subtracting low order tidal harmonic fit from the raw data that has a 1-min. sampling interval. This detiding method is not perfect and the detided trace can have a small non-zero offset (typically about 1 cm or so) well before the actual tsunami arrival. We subtracted the non-zero offset from the detided trace such that the detided trace is more or less at the zero value well before the tsunami arrival.

### 3.2 February 27, 2010 Chile tsunami

During the 2010 Chile tsunami, the RIFT model was run in real-time using the USGS W-phase centroid moment tensor solution (for the W-phase method, see Kanamori and Rivera, 2008; Hayes et al, 2009). The parameters used are: magnitude  $M_w=8.8$  ( $M_0=2.0 \times 10^{22}$  Nm), centroid 35.826 S, 72.668 W, Depth=35 km, strike=16, dip=14, rake=104. The length and width of the fault are 483.1 km and 99.5 km, respectively. With a shear modulus of 45 GPa, the uniform slip is 9.22 m. We were able to obtain real-time Pacific-wide propagation solution before the tsunami wave reached the nearest live DART 32412 (Foster et al. 2012). Unfortunately, the RIFT model was only integrated for 24 hours during the event, just before the tsunami peak arrival at the farthest DART (52405), so we reran the model for 30 hours for this study, using exactly the same parameters we used during the event. The results are the same except that we now have a longer time series. We label this run as “without depth-correction”. To implement the dispersion relation (4), we ran RIFT with exactly the same forcing used during the event, but the ocean depth was replaced by the effective depth, defined by (5). We label this run as “with depth-correction”.

Figure 4 compares the time series of model results without depth-correction (blue), with depth-correction (red), and the observed tsunami waveforms (black) at various DARTs across the Pacific. The DARTs are selected such that there is a good coverage of distance and azimuth (the locations and data of the DARTs can be found at NOAA’s National Data Buoy Center: <http://www.ndbc.noaa.gov/dart.shtml>. The locations of DART used are also plotted in Figure 6.). The DARTs are listed in the order of observed tsunami arrival times. Without depth-correction, the difference between the modeled and observed tsunami arrival times at the DARTs got progressively worse as the distance (in terms of tsunami travel time) from the epicenter increased (compare blue with black lines, Figure 4). With depth-correction (red), the difference is substantially reduced, compared to the model run without depth-correction (blue). The modeled tsunami arrival times now more or less match those of the observed at most of the DARTs (compare red and black lines), judging by the initial tsunami arrival, time of peak, or overall fit for later arriving waves.

For DART 51407 (near Hawaii, Figure 4h), the observed and modeled tsunami arrivals with depth-correction (red) are about the same, in contrast to the 8-min. discrepancy without depth-correction (blue, also see Figure 1c). The most dramatic improvement is for DART 52405. With depth-correction, the modeled waveform is now in phase with that of the observed, rather than being out of phase (Figure 4l, also see Figure 1e).

Despite the overall improvement of tsunami arrival time with depth-correction, there are significant differences between the modeled and observed tsunami waveforms at some DARTs. It is worth noting that the wave period of the modeled tsunami at DART 51406 is somewhat larger than that of the observed, such that the second peak does not line up with that of the observations (Figure 4b).

We note that the modeled waveform for DART 54401 differs significantly from that of the observed and the waveform without depth-correction seems match better overall to the observed,

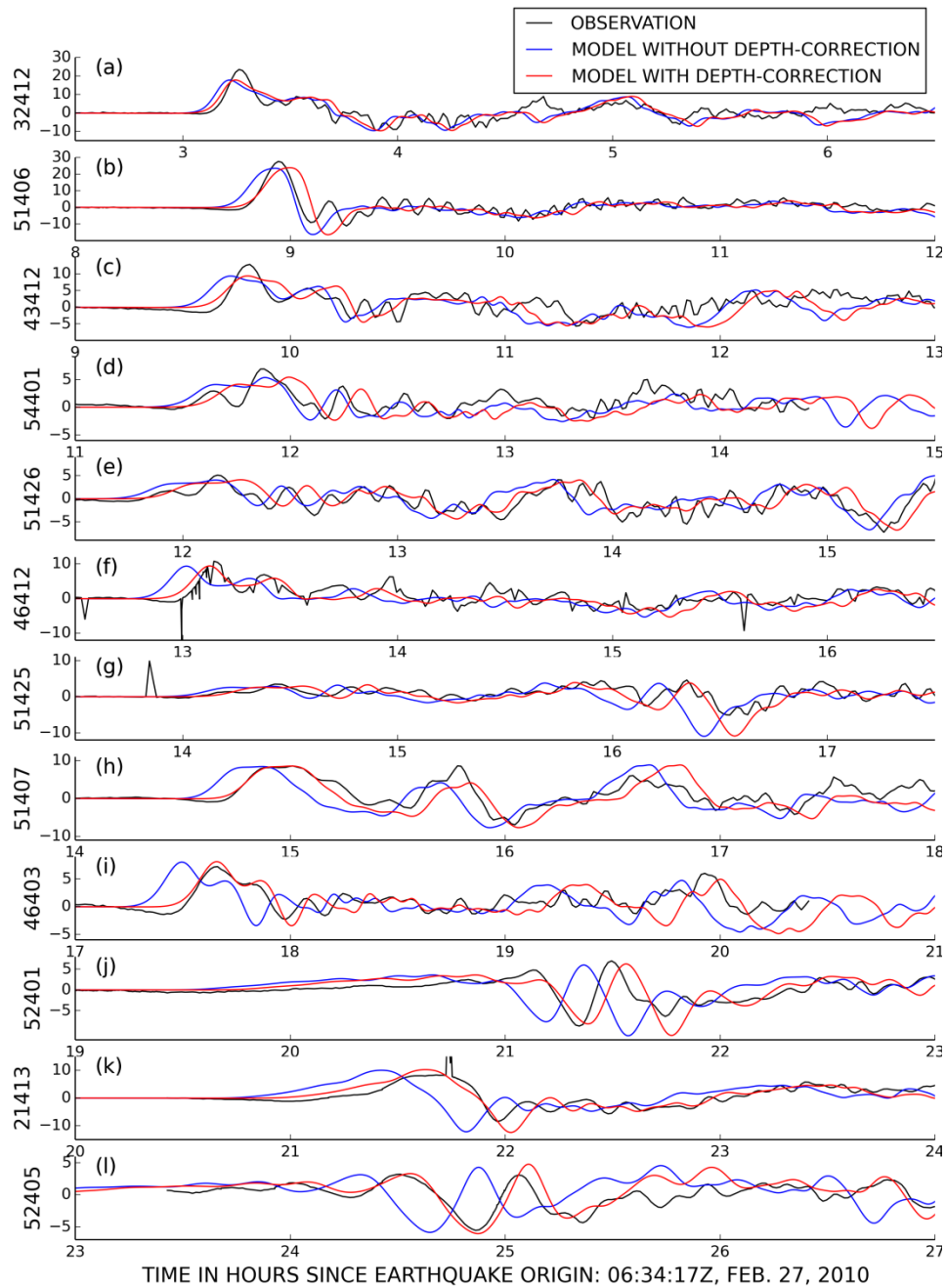


Figure 4. Comparison of model runs with (red) and without (blue) depth-correction with observations (black) at DARTs for the 2010 Chile tsunami. See Section 3.2 for details of forcing parameters used.

although with depth-correction, the initial arrival time seems to match the observation better (Figure 4d). The same can be said of DART 51246 (Figure 4e). The mismatch of the waves might be

attributable to the source model error. Even using a finite fault solution with DART inversion, Watada et al. (2014) was unable to reproduce the observed waveform at DART 51426.

It is worth noting that the first arriving waves are much smaller than later arriving waves at some DARTs. For example, maximum wave amplitudes occurred about two hours after the initial arriving waves at 51425 and 52401 (Figure 4g and Figure 4j). For these locations, it is more important that the modeled waveforms match the observed ones at the times of maximum wave amplitude. With depth-correction, the times of the maximum wave amplitudes do match better with the observed (near hour 16.3 for DART 51425 and near hour 21.5 for DART 52401. Figure 4g, j).

With depth-correction, it appears that only the phase of the tsunami wave is altered but the amplitude and shape of the tsunami remain unchanged. To take a closer look, we compare the model time series of sea level with and without depth-correction at the DARTs, shown in Figure 5. The time axis for the run without depth-correction is shifted from about 1 minute for the nearest DART (32412) to the epicenter to about 14 minutes for the farthest DART (52405). The time shifts needed to line up the model runs with and without depth-correction are also indicated in Figure 5. For the first few hours after the tsunami arrival, there is almost no difference between the time series with and without depth-correction, after adjusting for the tsunami arrival time. As time goes on, small differences begin to emerge. This is understandable because the difference in tsunami travel time will eventually have some effects on the wave fields, even in the open ocean, because travel time changes will lead to differential changes in wave reflection, scattering, and refraction, because of the complexities of the ocean bathymetry.

So far we only compared model results with and without depth-correction for a dozen DARTs. To get a sense of how depth-correction alters the tsunami wave basin wide, we show in Figure 6a,b the absolute difference and relative difference (percent) between the maximum wave amplitudes with and without depth-correction. The locations of the DARTs used for the comparison discussed above are also indicated (black triangles). The black square indicates the epicenter of the earthquake. For the vast areas of the deep open ocean, the absolute difference is less than 0.5 cm or relative difference is less than 10% (blue or cold color). Larger differences occur near the coastline and in areas where the depth is relatively shallow or in areas with complex topographic features, such as the low-latitude region of the western Pacific, the east of New Zealand, and the southwest Pacific. Differences as large as 100% are seen in the East China Sea. Large differences are also seen in the Arafura Sea (north of Australia). We need to point out that 30 hours of integration might not be long enough for waves to fully propagate into these regions. We should also note that tsunami waves in regions with water depth less than 500 m cannot be well resolved by the numerical model at 4-arc-min. resolution. For example, the wavelength for a 10-min. period wave for an ocean depth of 500 m is 42 km, covering only 5 to 6 model grid points. Thus, the numerical solution itself is questionable for these regions, where the water depth is only a few tens of meters. Interestingly, all the DARTs happened to be located in regions with small differences in percentage terms (Figure 6b).

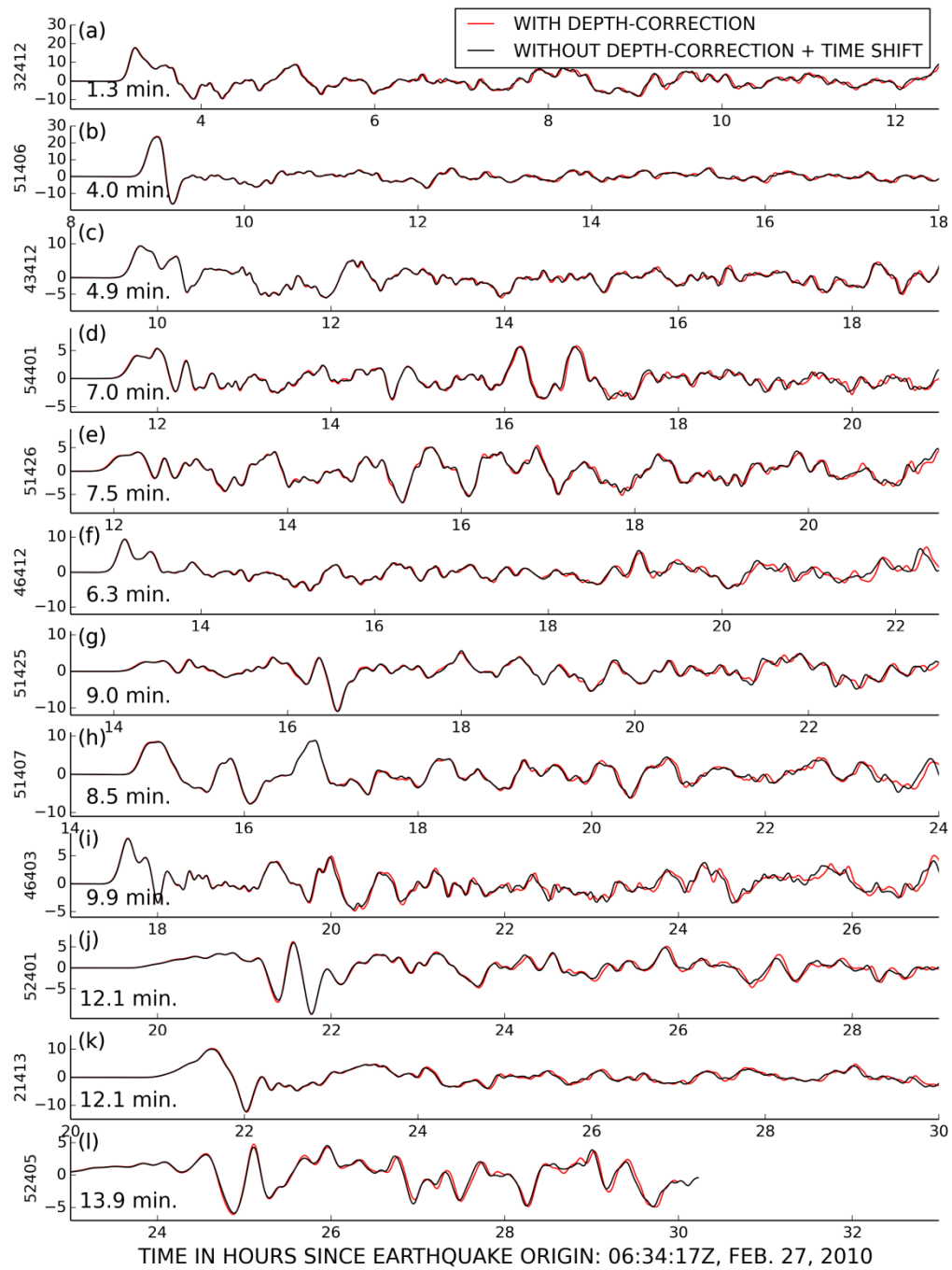


Figure 5 Comparison of model runs with (red) and without (black) depth-correction for the 2010 Chile Tsunami. The time axis for model run without depth-correction for each DART is shifted to line up the initial tsunami arrival with model run with depth-correction. The time shift varies from 1.3 min. for DART 32412 to 13.9 min. for DART 52405.

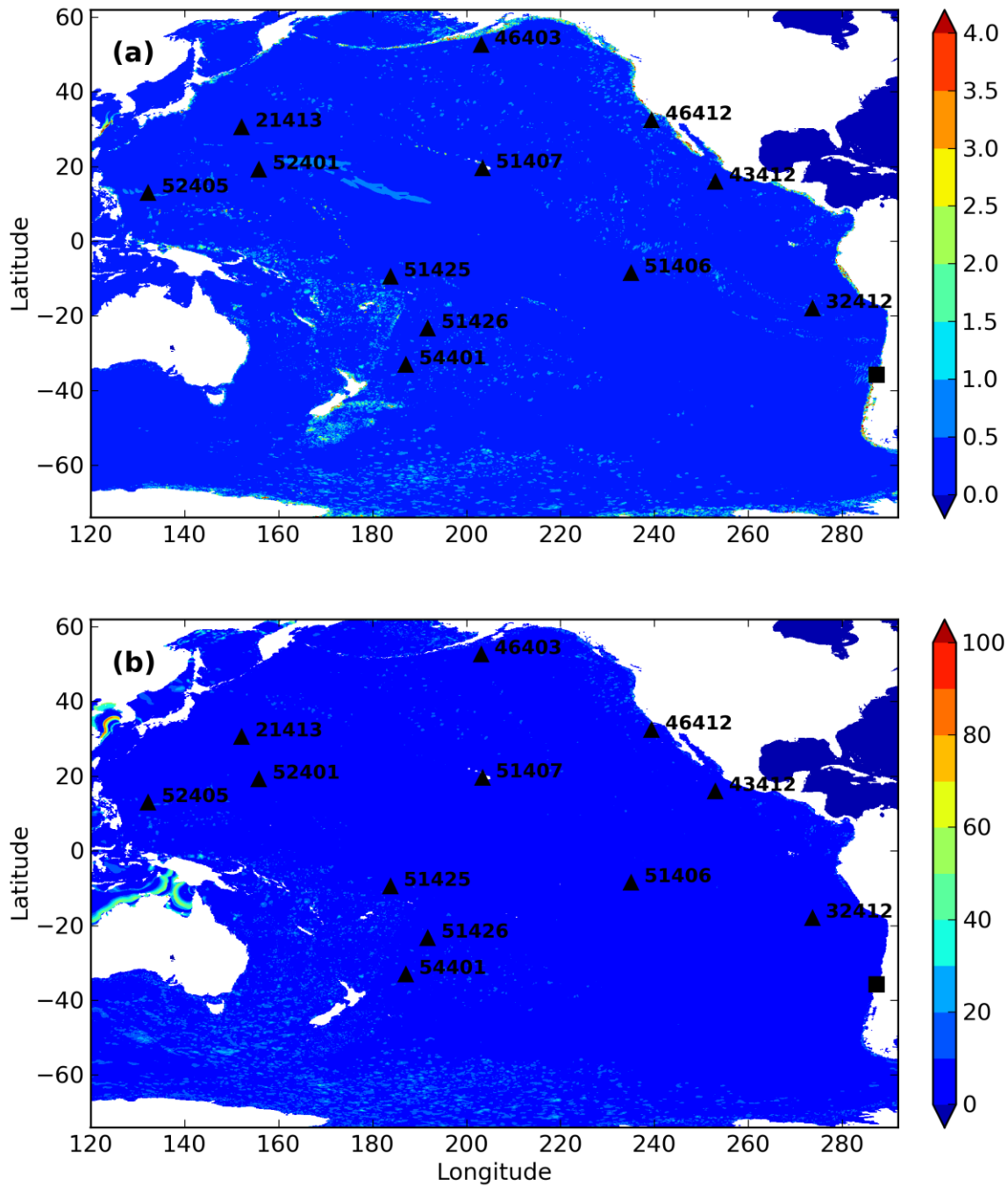


Figure 6 (a) Absolute difference (in cm) and relative difference (in percent) of maximum wave amplitude between model runs with and without depth-correction for the 2010 Chile tsunami. The locations of DARTs used in the model-observation comparison are also shown (black triangles). The Epicenter is indicated by the black square.

### 3.3 March 11, 2011 Tohoku tsunami

During the 2011 Tohoku tsunami, the RIFT model was run in real-time using a centroid moment tensor solution from the Global CMT Project (Dziewonski et al. 1981; Ekström et al. 2012, <https://www.ldeo.columbia.edu/research/seismology-geology-tectonophysics/global-cmt>), with a rectangular fault and uniform slip. The result was helpful during the event for PTWC's operations. Unfortunately, the result is not suitable for this travel time study, because even the tsunami arrival time at the nearest DART (21418) was several minutes earlier than that of the observed. This difference cannot be corrected by the depth-correction method. This suggests that a uniform slip of a rectangular fault is too crude to represent the sources of the Tohoku tsunami. We therefore forced the RIFT model with the USGS finite fault solution for this study. The USGS finite fault solution consists of 325 25-km by 20-km sub-faults, with a total fault area of 625 km by 260 km. ([http://earthquake.usgs.gov/earthquakes/eqinthenews/2011/usc0001xgp/finite\\_fault.php](http://earthquake.usgs.gov/earthquakes/eqinthenews/2011/usc0001xgp/finite_fault.php)). The rupture time of the sub-faults varies from 14 to 230 seconds and the rise-time varies from 9 to 26 seconds. This sub-fault solution amounts to a moment magnitude of 9.0.

Figure 7 compares model results without depth-correction (blue), with depth-correction (red), and observation (black) at DARTs. Again, the DARTs are selected to have a good coverage of distance and azimuth. Without depth-correction, the difference between the modeled and observed tsunami arrival times at the DARTs got progressively worse as the distance from the epicenter increased (compare blue and black curves). With depth-correction (red), the difference is substantially reduced, compared to the model run without depth-correction. For DART 21418, the tsunami waveforms with and without depth-correction showed little difference (Fig. 7a). This is because the DART is only a few hundred km from the source region. The tsunami arrived at DART 52405 after about 3.5 hours (Fig. 7c). At first glance, the model results with and without depth-correction do not seem to show much difference. A closer look however, reveals the arrival times differ by about 3 min, judging by the times of the peak tsunami amplitude.

The modeled tsunami still arrives 2-4 min. too soon compared to the observed for the furthest DARTs (43412, 32412, 32401, see Figure 7j, k, l), although the discrepancies are reduced substantially compared to the case without depth-correction. For example, without depth-correction, the second peak of the modeled tsunami at DART 32401 almost lines up with the first peak of the observed (compare blue and black in Figure 7l), whereas with depth-correction, the first peak from the model lines up with the observed first peak much better (compare red and black in Figure 7l).

For the 2011 Tohoku tsunami, the depth-correction approach cannot fully explain the discrepancies between the modeled and observed tsunami arrival times. We note some important differences between the two tsunamis. Although the Tohoku tsunami was generated by a larger earthquake, magnitude 9.0 vs. magnitude 8.8, the wave periods are somewhat shorter, as revealed in the spectral analysis of Yamazaki et al. (2011; 2012). Physical dispersion, which is lacking in our model, might have some effects on the modeled tsunami arrival times and might explain part of the remaining discrepancies. We also note we assumed the seafloor deformation is instantly translated to the sea surface deformation. In reality, there might be a finite time of adjustment. So the true discrepancies between the observed and modeled tsunami arrival times might be smaller than shown.

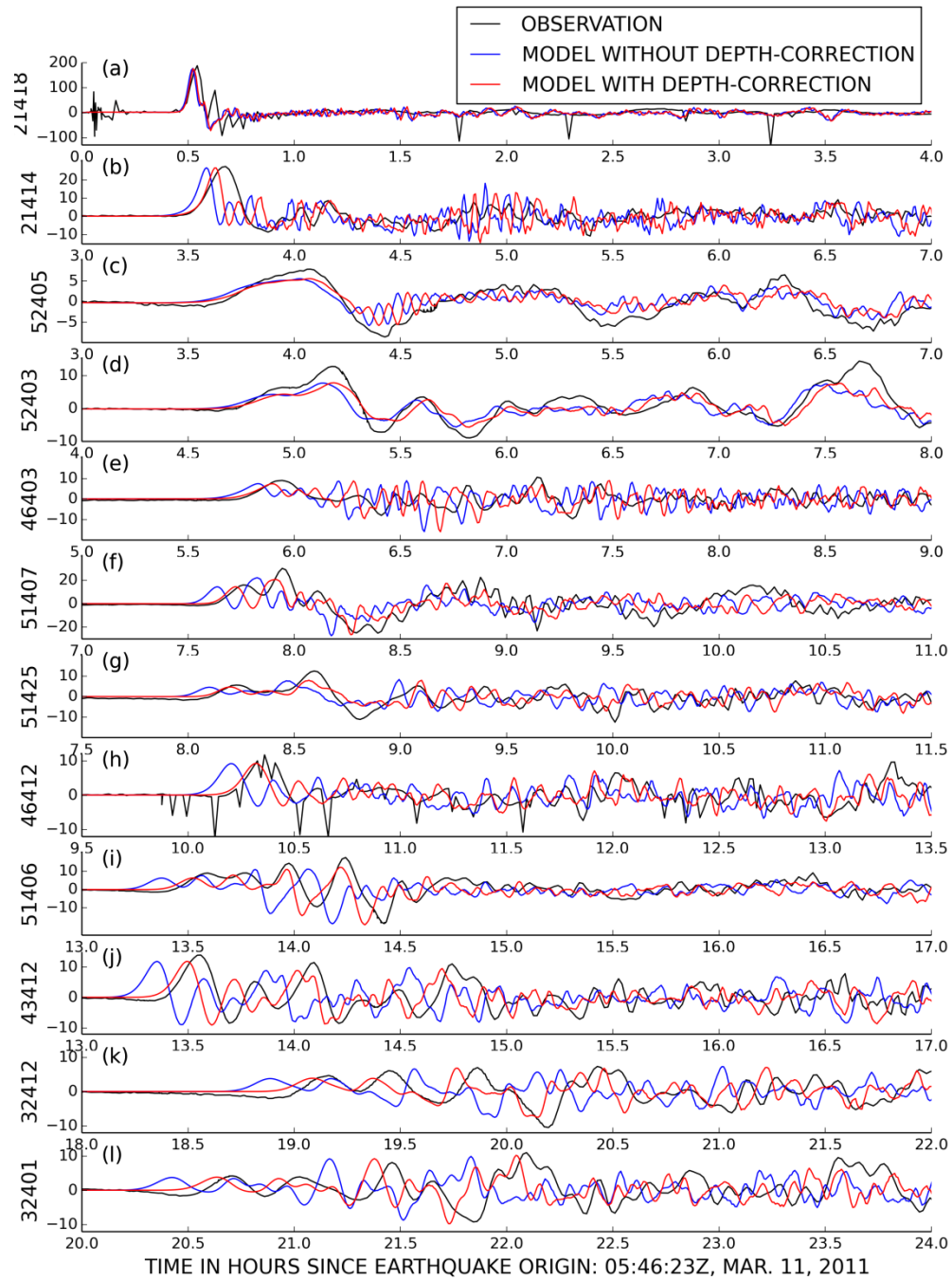


Figure 7. Comparison of model runs with and without depth-correction with observations at DARTs for the 2011 Tohoku tsunami. See Section 3.2 for details of forcing parameters used.

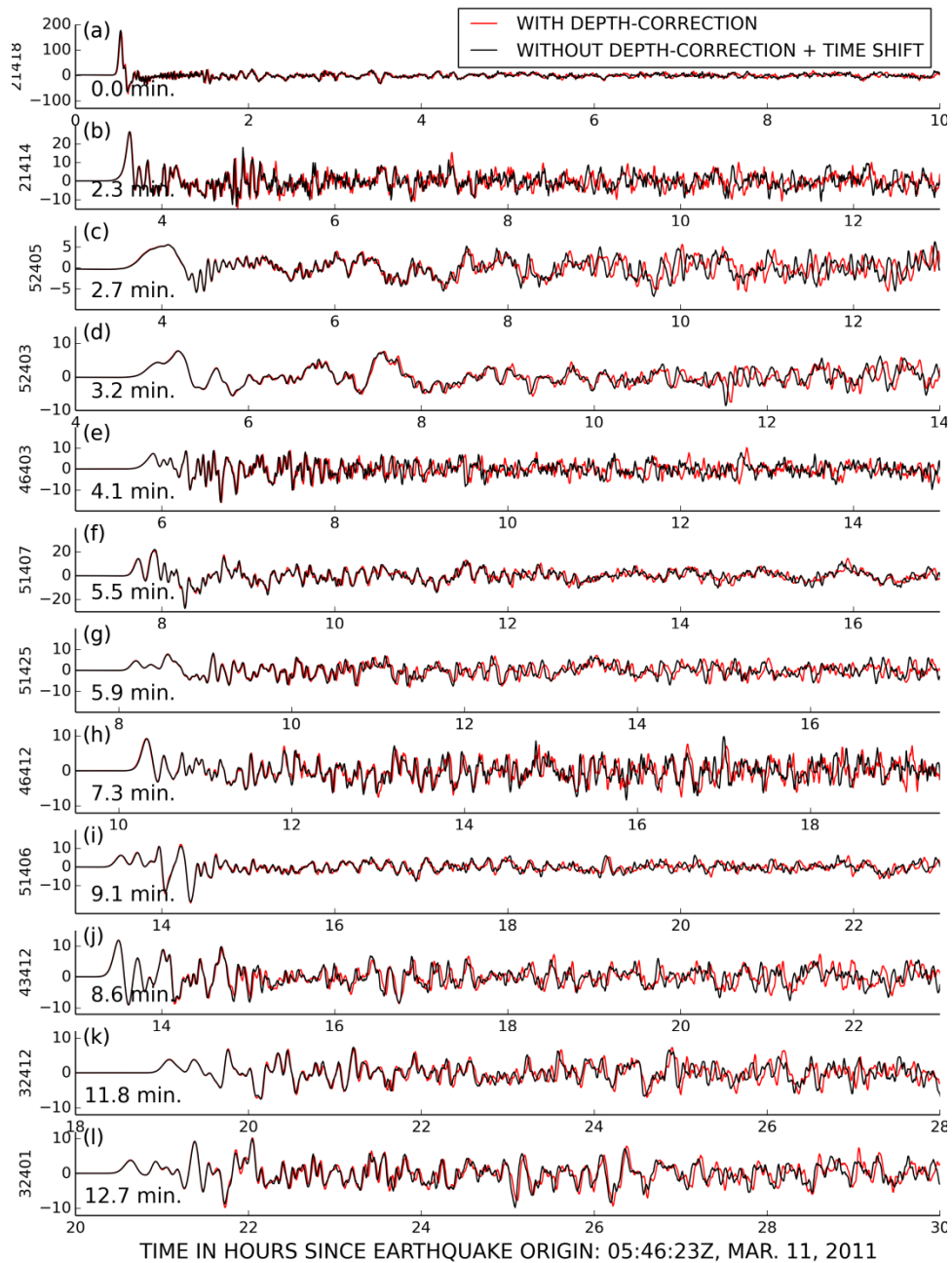


Figure 8. Comparison of model runs with (red) and without (black) depth-correction, for the Tohoku 2011 tsunami. The time axis for model run without depth-correction is shifted to line up the initial tsunami arrival with the model run with depth-correction. The time shifts (in minutes) needed to line up the two runs are indicated in the plots.

As for the case of 2010 Chile tsunami, we want to know whether or not depth-correction alters the tsunami wave forms, other than shifting the tsunami arrival times. Figure 8 compares the time series of model results at the DARTs with and without depth-correction. The time axis of the model run without depth-correction is shifted between 0 and 13 min. to line up with the tsunami arrival times of the model run with depth-correction (the time shifts are listed in Figure 8).

For the first two hours, there is almost no difference between the two model runs, after adjusting the time axis. Once again, depth-correction does little to the early direct arriving tsunami waves in the deep ocean other than shifting the tsunami arrival times. But as time goes on, the differences begin to appear. At DART 46403, for example, the waveforms with and without depth-correction have substantial differences (Figure 8e, near hour 13). Similar patterns can be seen at other DARTs.

Figure 9a, b show the absolute and relative difference of the maximum wave amplitude between the two model runs with and without depth-correction. The locations of the DARTs used for the comparison are also indicated (black triangles). The black square indicates the epicenter of the earthquake. For most areas of the open deep ocean, the difference is less than 1 cm (blue or cold color) or less than 10% in percentage terms. Again, larger differences occur near the coastline and in areas where the depth is shallow or in areas with complex topographic features, such as the low-latitude region of the western Pacific and east of New Zealand. Relatively large differences can also be seen in some areas of the deep ocean. For example, the differences are about a 3-4 centimeters near the Kuril Trench and off the east coast of Japan (Figure 9a, upper-left corner). Overall, the absolute difference is larger than that of the 2010 Chile tsunami (compare Figure 6a and Figure 9a). The relative difference (percentage-wise) however, is rather similar. Note the elevated absolute difference shown near Kuril Trench and along the great circle from Japan to South America do not show up in relative difference (compare Figure 9a with Figure 9b). For the southern ocean, the 2011 Tohoku tsunami does show somewhat larger relative difference, up to 30-40% (south of Australia). The regions of large differences are fragmented and mixed with regions of small differences (e.g., south of Australia). Again, at 4-arc-min. resolution, our model cannot resolve tsunami waves in shallow waters. The difference between model runs with and without depth-correction in areas with an ocean depth less than 500 m will not be very meaningful. Much higher resolution or nested-grid approach is needed to further study the true effects of depth-correction in shallow waters.

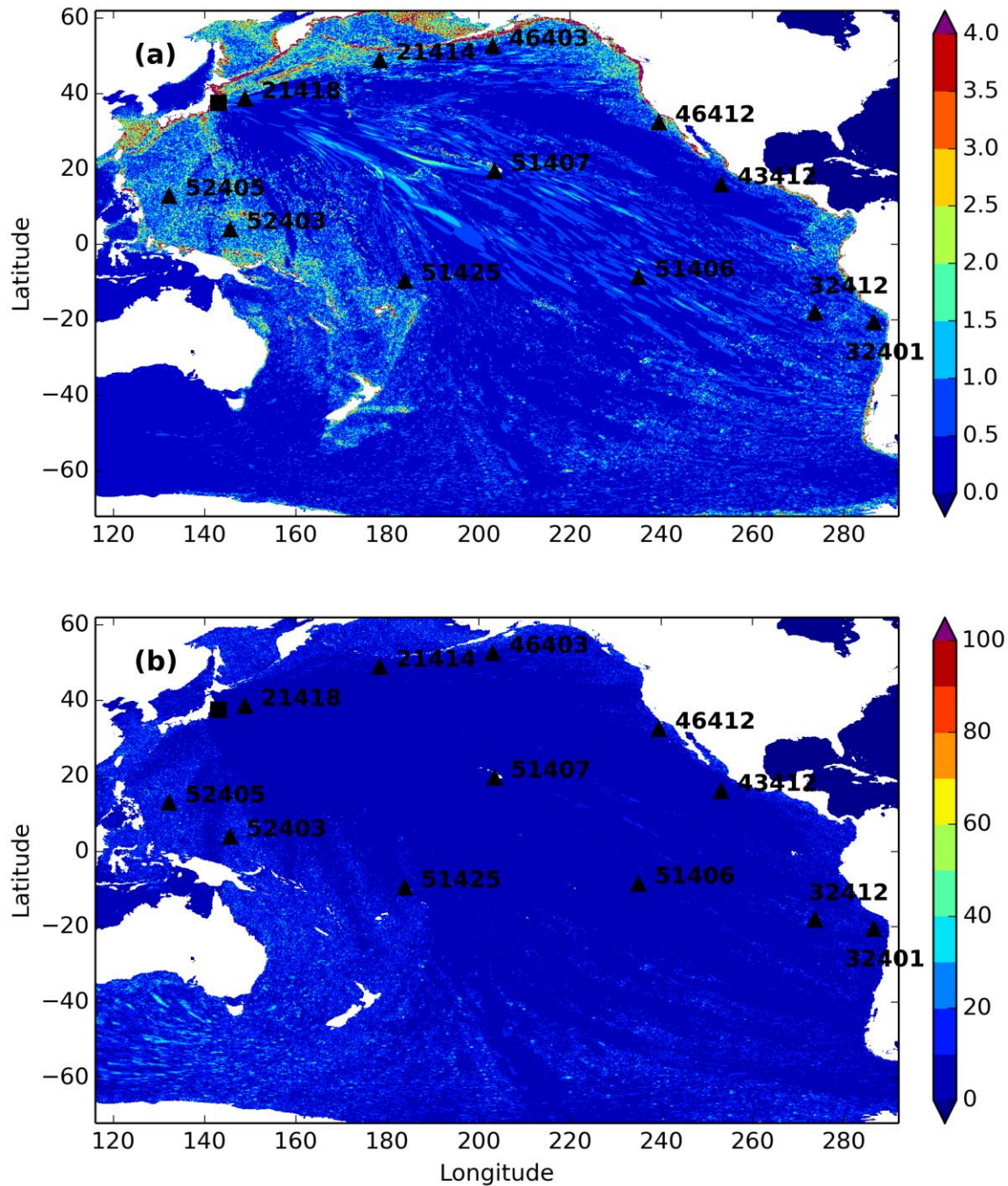


Figure 9. (a) Absolute difference (in cm) and (b) relative differences (in percent) of maximum wave amplitude between model runs with and without depth-correction for the 2011 Tohoku tsunami (unit: cm). The locations of DARTs used in the model-observation comparison are also shown (black triangles). The Epicenter is indicated by the black square.

#### 4. Conclusions

We proposed a simple ocean depth-correction method to reduce the discrepancies of the modeled and observed tsunami arrival times. The method is based on the dispersion relation of shallow water surface gravity waves in a compressible homogenous fluid. The phase speed of surface gravity waves is reduced in such a system. Implementation of this method is straightforward by replacing the ocean bathymetry used in numerical models by the effective bathymetry, according to formula (5). There is no need to modify the numerical codes of the existing tsunami models (i.e., there is no extra computational cost). Although our method does not take into account the full physics of the interaction of the ocean and the elastic earth, it can be interpreted as a bulk-parameterization of these effects. We applied this approach to the 2010 Chile and 2011 Tohoku tsunamis with forcing purely derived from seismic data and found that the depth-correction can account for most of the discrepancies between the modeled and observed tsunami arrival times. Discrepancies of 3-4 min. still remain for the 2011 Tohoku tsunami.

The depth-correction approach did not seem to alter the behavior of the direct arriving tsunami waves (waveforms and amplitudes) at DARTs within a couple hours of tsunami arrival, other than shifting the tsunami arrival times to match better with observations. However, substantial differences still occur in regions of shallow water and regions of complex bathymetry. This depth-correction method can potentially be used to improve the accuracy of tsunami source inversion by improving tsunami arrival times at far field DARTs. Basin wide, the differences between runs with and without depth-correction are less than 10% over most part of the deep ocean. To accurately assess the effects of depth-correction on coastal run-ups however, resolution capable of resolving inundation is needed.

Errors in model tsunami arrival times can arise from the inaccuracies of the source models. For example, Allgeyer and Cummins (2014) showed that source models derived from fitting model to observed tsunamis result in smaller tsunami travel time errors. Errors in model numerics can also contribute to the tsunami arrival time error. Shallow water equations might not be suitable for events with short tsunami wave periods or wavelengths. Most if not all tsunami forecast models (for warning purposes, at least) in use today are based on shallow water equations, without resolving the physical dispersion of tsunami waves. Different numerical codes can also have different characteristics of numerical errors (numerical dispersion and dissipation, etc.). Even if the same travel time correction method is used, the numerical results from different models might be different.

As a final remark, we note that although the depth-correction method proposed in this study is simple and easy to implement, it has its limitations because it does not account for the full physics that affect tsunami travel time. We were not able to reproduce the small initial depression observed (although the small initial depression is of no consequence as far as tsunami warning is concerned). However, taking into account fully the physics influencing tsunami travel time might require integrating a coupled ocean and elastic earth system. The ocean component of the coupled system might have to be a non-hydrostatic, compressible, and baroclinic ocean model or a model capable of representing these effects. Such a coupled model will be unfeasible for the foreseeable future, at least for tsunami warning purposes.

## Acknowledgements

We thank Dr. Stuart Weinstein and Dr. Gerard Fryer of PTWC for helpful discussions and comments. We thank the National Data Buoy Center (NDBC) for maintaining the DART network and for providing the DART data. We also thank Gavin Hayes of US Geological Survey for providing the W-phase CMT solution for the 2010 Chile earthquake and the finite fault solution of the 2011 Tohoku earthquake. Editorial assistance from Juleen Wong is greatly appreciated.

## References

- Allgeyer, S. and P. Cummins (2014), Numerical tsunami simulation including elastic loading and seawater density stratification, *Geophys. Res. Lett.*, 41, doi:10.1002/2014GL059348.
- Arakawa, A. and V. Lamb (1977): Computational design of the basic dynamical processes of the UCLA general circulation model, *Methods in Computational Physics*, Vol. 17, 174-267.
- Becker, J. J., D. T. Sandwell, W. H. F. Smith, J. Braud, B. Binder, J. Depner, D. Fabre, J. Factor, S. Ingalls, S-H. Kim, R. Ladner, K. Marks, S. Nelson, A. Pharaoh, R. Trimmer, J. Von Rosenberg, G. Wallace and P. Weatherall (2009): Global Bathymetry and Elevation Data at 30 Arc Seconds Resolution: SRTM30\_PLUS, *Marine Geodesy*, 32:4, 355-371, DOI: 10.1080/01490410903297766
- Dziewonski, A. M., T.-A. Chou and J. H. Woodhouse, Determination of earthquake source parameters from waveform data for studies of global and regional seismicity, *J. Geophys. Res.*, 86, 2825-2852, 1981. doi:10.1029/JB086iB04p02825
- Ekström, G., M. Nettles, and A. M. Dziewonski (2012): The global CMT project 2004-2010: Centroid-moment tensors for 13,017 earthquakes, *Phys. Earth Planet. Inter.*, 200-201, 1-9. doi:10.1016/j.pepi.2012.04.002
- Foster, J. H., B. A. Brooks, D. Wang, G. S. Carter and M. A. Merrifield (2012): Improving Tsunami Warning Using Commercial Ships. *Geophys. Res. Lett.*, doi:10.1029/2012GL051367
- Grilli, S. T., J.C. Harris, T. S. T. Bakhsh, T. L. Masterlark, C. Kyriakopoulos, J.T. Kirby, and F. Shi (2012): Numerical simulation of the 2011 Tohoku tsunami based on a new transient FEM co-seismic source: Comparison to far- and near-field observations, *Pure Appl. Geophys.*, doi:10.1007/s00024-012-0548-y.
- Hayes, G. P., L. Rivera, and H. Kanamori (2009): Source inversion of W phase: Real time implementation and extension to low magnitudes, *Seismol. Res. Lett.*, 80(5), 817-822, doi:10.1785/gssrl.80.5.817.

- Inazu, D. and T. Saito (2013): Simulation of distant tsunami propagation with a radial loading deformation effect, *Earth Planets Space*, Vol. 65, 835-842.
- Kanamori, H. and L. Rivera (2008): Source inversion of W phase: Speeding up seismic tsunami warning, *Geophys. J. Int.*, 175, 222–238, doi:10.1111/j.1365-246X.2008.03887.x.
- Kato, T., Y. Terada, H. Nishimura, T. Nagai and S. Koshimura (2011): Tsunami records due to the 2010 Chile Earthquake observed by GPS buoys established along the Pacific coast of Japan. *Earth, Planets, and Space*, 63, e5–e8.
- Kono, Y., S. Takata, F. Imamura, K. Minoura (2002): Numerical Analysis on Johgan Tsunami by Using Fault Model in Consideration of the Origin of Miyagi-Ken-Oki Earthquake. The 5<sup>th</sup> International Conference on Hydro-Science and Engineering, Warsaw, Poland, September 2002.
- Okada, Y. (1985): Surface deformation due to shear and tensile faults in a half space, *Bull. Seismol. Soc. Am.*, Vol. 75, 1135-1154.
- Okal, E. A. (1982): Mode-wave equivalence and other asymptotic problems in tsunami theory. *Phys. Earth Planet. Inter.*, Vol. 30, 1-11.
- Ray, R.D. (1998): Ocean self-attraction and loading in numerical tidal models, *Marine Geodesy*, Vol. 21, No. 3, 181-192, DOI: 10.1080/01490419809388134
- Saito, T., Y. Ito, D. Inazu and R. Hino (2011): Tsunami source of the 2011 Tohoku - Oki earthquake, Japan: Inversion analysis based on dispersive tsunami simulations, *Geophys. Res. Lett.*, 38, L00G19, doi:10.1029/2011GL049089.
- Shchepetkin, A. F. and J. C. McWilliams (2011): Accurate Boussinesq oceanic modelling with a practical, “stiffened” equation of state. *Ocean Modelling*, Vol. 38, pp. 41-70.
- Tsai V.C., J.P. Ampuero J.P., Kanamori H., and D.J. Stevenson D.J., (2013): Estimating the effect of Earth elasticity and variable water density on tsunami speeds. *Geophys. Res. Lett.*, Vol. 40, 492-496, doi:10.1002/grl.50147.
- Wang, D., D. Walsh, N. Becker, and G. Fryer (2009): A methodology for tsunami wave propagation forecast in real time, *EOS Trans AGU*, 90(52), Fall Meet. Suppl., Abstract OS43A-1367.
- Wang, D., et al. (2012), Real-time forecasting of the April 11, 2012 Sumatra tsunami, *Geophys. Res. Lett.*, 39, L19601, doi:10.1029/2012GL053081.

- Ward, S. N. (1980): Relationships of tsunami generation and an earthquake source. *J. Phys. Earth*, vol. 28, 441-474.
- Watada, S., K. Satake, Y. Fujii (2011): Origin of traveltime anomalies of distant tsunami, in Abstract NH11A-1363 presented at 2011 Fall Meeting, AGU, San Francisco, Calif., 5-9 Dec
- Watada, S. (2013), Tsunami speed variations in density-stratified compressible global oceans, *Geophys. Res. Lett.*, 40, 4001-4006, doi:10.1002/grl.50785.
- Watada, S., S. Kusumoto, and K. Satake, (2014): Traveltime delay and initial phase reversal of distant tsunamis coupled with the self-gravitating elastic earth. *J. Geophys. Res., Solid Earth*, Vol. 119, No. 5, pp. 4287–4310, DOI: 10.1002/2013JB010841.
- Wells, D. L. and K. J. Coppersmith (1994), New empirical relationships among magnitude, rupture length, rupture width, rupture area, and surface displacement, *Bull. Seismol. Soc. Am.*, Vol 84, 974-1002.
- Yamamoto, T. (1982), Gravity waves and acoustic waves generated by submarine earthquakes, *Intl. J. Soil Dyn. Earthq. Eng.*, 1, 75-82.
- Yamazaki, Y., K. F. Cheung (2011): Shelf resonance and impact of near-field tsunami generated by the 2010 Chile earthquake. *Geophys. Res. Lett.*, Vol. 38, L12605, doi:10.1029/2011GL047508.
- Yamazaki, Y., K. F. Cheung, G. Pawlak and T. Lay (2012): Surges along the Honolulu coast from the 2011 Tohoku tsunami, *Geophys. Res. Lett.*, 39, L09604, doi:10.1029/2012GL051624.
- Yasuda, T. and H. Mase (2013): Real-time tsunami prediction by inversion method using offshore observed GPS buoy data: Nankaido. *J. Waterways, Port, Coastal, and Ocean Engineering*, Vol. 139, No. 3, pp. 221-231.